CHEMISTRY OF MATERIALS

Article

pubs.acs.org/cm

Dibenzothiophene-Based Phosphine Oxide Host and Electron-Transporting Materials for Efficient Blue Thermally Activated Delayed Fluorescence Diodes through Compatibility Optimization

Chaochao Fan,[†,§] Chunbo Duan,[†,§] Ying Wei,[†,‡] Dongxue Ding,[†] Hui Xu,*[,†,‡] and Wei Huang*[,‡]

[†]Key Laboratory of Functional Inorganic Material Chemistry, Ministry of Education, Heilongjiang University, 74 Xuefu Road, Harbin 150080, P. R. China

[‡]Key Laboratory of Flexible Electronics (KLOFE) & Institute of Advanced Materials (IAM), Jiangsu National Synergistic Innovation Center for Advanced Materials (SICAM), Nanjing Tech University (NanjingTech), 30 South Puzhu Road, Nanjing 211816, P.R. China

Supporting Information

ABSTRACT: Thermally activated delayed fluorescence (TADF) organic light-emitting diodes arise from the development of high-performance host materials and carrier transporting materials fitting for TADF dyes with optimized respective properties and interplays, making simultaneous performance improvement and device structure simplification feasible. In this work, a highly efficient blue TADF diode with simplified four-layer structure was successfully achieved by utilizing bis[4-(9,9-dimethyl-9,10-dihydroacridine)-phenyl]sulfone (**DMAC-DPS**) as blue emitter, 4,6-bis(diphenylphosphoryl)-dibenzothiophene (**DBTDPO**) as host, and 4,6-bis(diphenylphosphoryl)-dibenzothiophene sulfone (**46DBSODPO**) as electron-transporting layer. The compatibilities between **DBTDPO** and **DMAC-DPS** and **DBTDPO** and **46DBSODPO** were optimized with respect to configuration, polarity, energy level, and interfacial interaction, resulting in the unchanged roughness of ~0.25 nm before and after doping, high photoluminescence quantum yield over 85%, and reduced interfacial exciplex emissions. With the similar triplet excited energy (T_1) of ~3.0 eV but inferior electrical properties compared to its analogues **28DBSODPO** and **37DBSODPO**, besides the homogeneity with **DBTDPO**, **46DBSODPO** suppressed the formation of interfacial exciplex and dipole for efficient exciton confinement and electron injection and transportation, in virtue of the steric effects of its *ortho*-substituted phosphine oxide groups. Consequently, **DBTDPO** and **46DBSODPO** endowed their **DMAC-DPS** based four-layer devices with the state-of-the-art performance, for example, the maximum external quantum efficiency over 16%, which was more than two-fold of those of conventional electron-transporting material 1,3,5-tri[(3-pyridyl)-phen-3-yl]benzene (**TmPyPB**). This design strategy about material compatibility could pave a way for developing high-performance blue TADF diodes with simplified configurations.

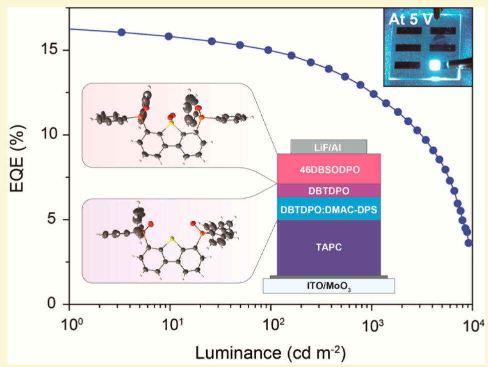

1. INTRODUCTION

After the success of phosphorescence organic light-emitting diodes (PHOLEDs) in harvesting both singlet and triplet excitons for 100% internal quantum efficiency,[1−3] recently, organic light-emitting diodes (OLEDs) employing pure-organic thermally activated delayed fluorescence (TADF) dyes achieve the same effect, in virtue of reverse intersystem crossing (RISC) induced triplet−singlet transformation.[4,5] Since efficient RISC requires small triplet−singlet energy splitting (ΔE_{ST}),[6,7] donor−acceptor (D−A) structure is mostly adopted to construct TADF dyes on account of the relatively low energy for the singlet charge transfer state ($^1CT^*$).[8−17] In this case, the large polarity of CT states[18,19] and the involvement of triplet exciton in electroluminescent (EL) process make suppression of emissive layer (EML)-inside[20,21] and interfacial quenching effects,[22] for example, concentration quenching (CQ),[23] triplet-polaron quenching (TPQ), and triplet−triplet annihilation (TTA),[24] crucial to realize high EL efficiencies. With this fundamental concern, EML compositions and interfacial effects of TADF devices should be rationally optimized through enhancing host-dopant and EML-carrier transporting layer (CTL) compatibility, making the development of high-performance host materials and carrier transporting materials (CTMs) fitting for TADF dyes imperative.[25−29]

A substantial challenge is addressed that the first triplet energy levels (T_1) of blue TADF dyes,[20,30−38] for example, bis[4-(9,9-dimethyl-9,10-dihydroacridine)phenyl]sulfone (**DMAC-DPS**, T_1 = 2.9 eV),[35] are remarkably higher than those of their phosphorescent counterparts, such as bis(4,6-(difluorophenyl) pyridinato-N,C^2)picolinate iridium(III)

Received: May 29, 2015
Revised: July 1, 2015

DOI: 10.1021/acs.chemmater.5b02012
Chem. Mater. XXXX, XXX, XXX−XXX

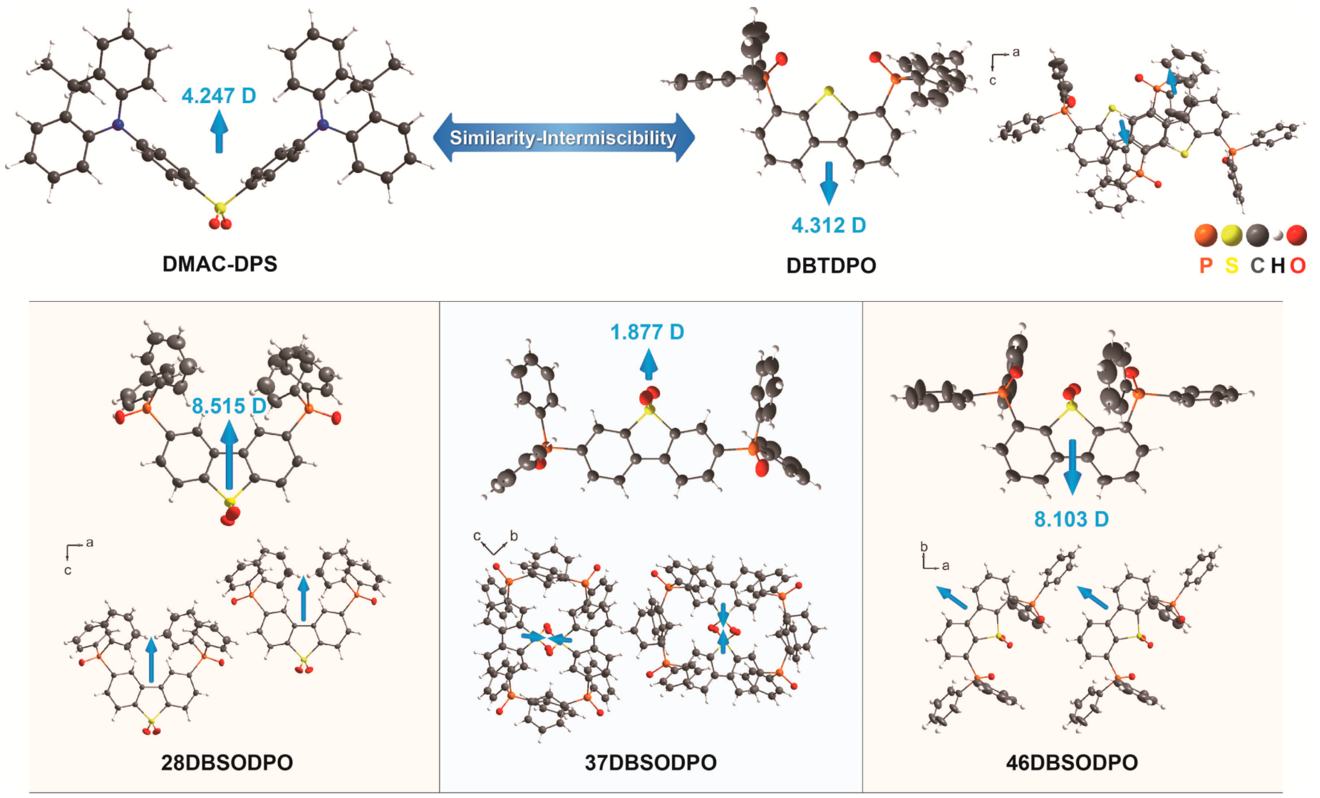

Figure 1. Molecular structures and packing diagrams of single crystals of **DBTDPO** and ***m*****DBSODPO** and their dipole moments in comparison with **DMAC-DPS**.

(**FIrpic**, T_1 = 2.7 eV)[39] even though their EL spectra are similar. Therefore, to confine exciton on **DMAC-DPS**, the requirement of optical properties for host materials and EML-adjacent CTMs is so severe that their T_1 values should be higher than or at least equivalent to 2.9 eV at the expense of electrical performance,[34,35] consequently forcing the employment of exciton-blocking and CTLs to accordingly suppress exciton diffusion and balance charge flux. As the result, the configuration of blue TADF devices was much more complicated than those of their green, yellow, and red analogues,[35] making it become one of bottlenecks of practical applications for TADF technology. Obviously, structural simplification of blue TADF devices can be established through taking both the own performance of each material and, especially, the intralayer and interlayer compatibilities into account.

Herein, we report a simplified highly efficient four-layer blue TADF diode utilizing 4,6-bis(diphenylphosphoryl) dibenzothiophene (**DBTDPO**) as host, its derivative 4,6-bis(diphenylphosphoryl) dibenzothiophene sulfone (**46DBSODPO**) as electron-transporting layer (ETL), and **DMAC-DPS** as dopant. Low driving voltages of <3 V for onset and <5.5 V at 150 cd m^{-2} and the state-of-the-art EQE of 16.1% for maximum and 14.7% and 12.4% at 150 and 1000 cd m^{-2} were realized. The consistent V-shape configuration and polarity of **DBTDPO** and **DMAC-DPS** and their well-matched optical properties rendered the unchanged morphology and stabilized T_1 states of **DMAC-DPS**-doped thin films with root−mean−square (RMS) roughness of ~0.25 nm, long delay-fluorescence lifetime of 11.5 μs, and high photoluminescence quantum yield (PLQY) more than 85%. In contrast to its constitutional isomers **28DBSODPO** and **37DBSODPO** (Figure 1 and Scheme 1), **46DBSODPO** is comparable in optical properties, for example, high T_1 of 2.97 eV for exciton diffusion suppression, but inferior in electron injection and transportation. Nevertheless, owing to the optimized compatibilities between **DBTDPO** and **46DBSODPO** in polarity, configuration, energy level, and interfacial interaction, the device efficiencies of **46DBSODPO** were more than 1.5-fold those of **28DBSODPO** and **37DBSODPO** and 2-fold those of a conventional high-T_1 electron-transporting material (ETM) 1,3,5-tri[(3-pyridyl)-phen-3-yl]benzene (**TmPyPB**). This contribution rationally demonstrated the significance of material compatibility for blue TADF diodes, especially when simplifying configurations without loss of performance.

2. EXPERIMENTAL SECTION

Materials and Instruments. All the reagents and solvents used for the synthesis were purchased from Aldrich and Acros companies and used without further purification. **DBTDPO** was prepared according to our previous report.[40]

^{1}H NMR spectra were recorded using a Varian Mercury plus 400NB spectrometer relative to tetramethylsilane (TMS) as internal standard. Molecular masses were determined by FINNIGAN LCQ electrospray ionization−mass spectrometry (ESI−MS) or matrix-assisted laser desorption ionization time-of-flight MS (MALDI-TOF-MS). Elemental analyses were performed on a Vario EL III elemental analyzer. Absorption and photoluminescence (PL) emission spectra of the target compound were measured using a SHIMADZU UV-3150 spectrophotometer and a SHIMADZU RF-5301PC spectrophotometer, respectively. Thermogravimetric analysis (TGA) and differential scanning calorimetry (DSC) were performed on Shimadzu DSC-60A and DTG-60A thermal analyzers under nitrogen atmosphere at a heating rate of 10 °C min^{-1}. Cyclic voltammetric (CV) studies were conducted using an Eco Chemie B. V. AUTOLAB potentiostat in a typical three-electrode cell with a platinum sheet working electrode, a

DOI: 10.1021/acs.chemmater.5b02012
Chem. Mater. XXXX, XXX, XXX−XXX

Scheme 1. Synthetic Procedure of *m*DBSODPO

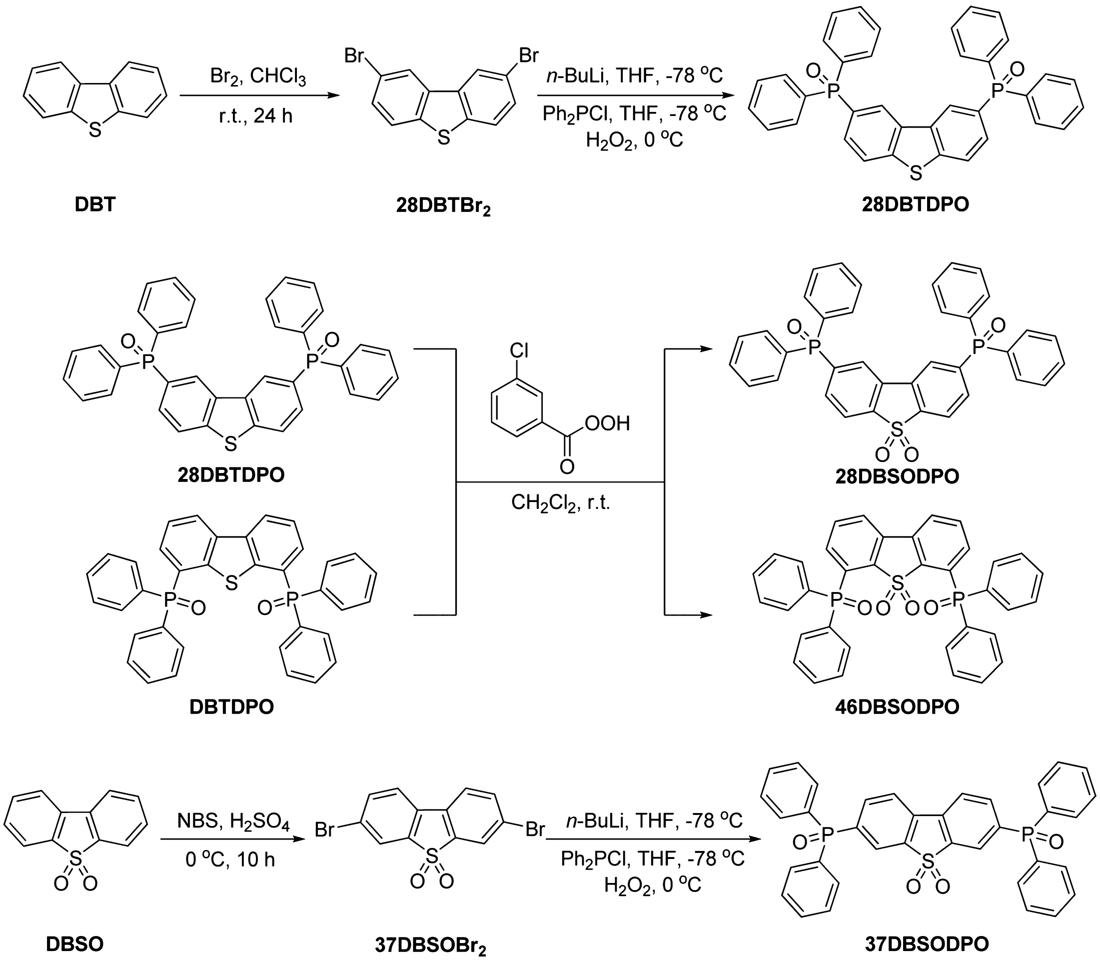

platinum wire counter electrode, and a silver/silver nitrate (Ag/Ag^+) reference electrode. All electrochemical experiments were carried out under a nitrogen atmosphere at room temperature in dichloromethane. Phosphorescence spectra were measured in dichloromethane using an Edinburgh FPLS 920 fluorescence spectrophotometer at 77 K cooling by liquid nitrogen with a delay of 300 μs using time-correlated single photon counting (TCSPC) method with a microsecond pulsed Xenon light source for 10 μs−10 s lifetime measurement, the synchronization photomultiplier for signal collection, and the multichannel scaling mode of the PCS900 fast counter PC plug-in card for data processing.

Synthesis of 2,8-Dibromodibenzothiophene (28DBTBr$_2$). In Ar$_2$, 1.84 g of dibenzothiophene (**DBT**, 10 mmol) was dissolved in 20 mL of chloroform, and then 1.54 mL of Br$_2$ (30 mmol) was added. The mixture was stirred for 24 h at room temperature. The reaction was quenched by addition of aq. NaHSO$_3$ (4 mL) and extracted by dichloromethane (3 × 2 mL). The organic layer was combined and dried with anhydride Na$_2$SO$_4$. The solvent was removed in vacuo. The residue was purified by flash column chromatography to afford 1.4 g of white powder with a yield of 40%. ^{1}H NMR (TMS, CDCl$_3$, 400 M Hz): δ = 8.233 (s, 2H), 7.699 (d, J = 8.4 Hz, 2H), 7.591 ppm (d, J = 8.4 Hz, 2H). LDI-TOF: m/z (%): 342 (100) [M$^+$]; elemental analysis (%) for C$_{12}$H$_6$Br$_2$S: C 42.14, H 1.77, S 9.37; found: C 42.15, H 1.79, S 9.42.

2,8-Bis(diphenylphosphoryl)dibenzothiophene (28DBTDPO). In Ar$_2$, 0.34 g of **28DBTBr$_2$** (1 mmol) and 1.3 mL of *n*-BuLi (2.5M, 3.25 mmol) in 15 mL of THF were mixed and stirred at −78 °C for 2 h. Then, 0.9 mL of Ph$_2$PCl (4.77 mmol) was added to the system at −78 °C and stirred for 8 h. The reaction was quenched by addition of water (4 mL) and extracted by dichloromethane (3 × 2 mL). The organic layer was dried with anhydride Na$_2$SO$_4$. The solvent was removed in vacuo. The residue was purified by flash column chromatography to afford 0.35 g of white powder with a yield of 50%. ^{1}H NMR (TMS, CDCl$_3$, 400 M Hz): δ = 8.476 (d, J = 12.4 Hz, 2H), 7.969 (d, J = 6.8 Hz, 2H), 7.781 (t, J = 9.6 Hz, 2H), 7.714 (q, J_1 = 7.6, J_2 = 12.0 Hz, 8H), 7.581 (t, J = 7.2 Hz, 4H), 7.490 ppm (t, J = 6.2 Hz, 8H). LDI-TOF: m/z (%): 584 (100) [M$^+$]; elemental analysis (%) for C$_{36}$H$_{26}$O$_2$P$_2$S: C 73.96, H 4.48, S 5.48; found: C 73.94, H 4.50, S 5.53.

General Procedure of Oxidation for Sulphone. A sample of 0.584 g of **DBT** phosphine oxide derivative (1 mmol) was dissolved into 10 mL of dichloromethane at room temperature, and then 0.86 g of 3-chlorobenzoperoxoic acid (5 mmol) was added to the mixture and stirred for 6 h. The reaction was quenched by addition of water (5 mL) and extracted by dichloromethane (3 × 2 mL). The organic layer was dried with anhydride Na$_2$SO$_4$. The solvent was removed in vacuo. The residue was purified by flash column chromatography.

2,8-Bis(diphenylphosphoryl)dibenzothiophene Sulfone (28DBSODPO). A sample of 0.35 g of white powder with a yield of 57%. ^{1}H NMR (TMS, CDCl$_3$, 400 M Hz): δ = 8.262 (d, J = 11.6 Hz, 2H), 7.912 (d, J = 8.0 Hz, 2H), 7.795 (t, J = 9.4 Hz, 2H), 7.612 (m, 12H), 7.517 ppm (t, J = 7.4 Hz, 8H). LDI-TOF: m/z (%): 616 (100) [M$^+$]; elemental analysis (%) for C$_{36}$H$_{26}$O$_4$P$_2$S: C 70.12, H 4.25, S 5.20; C 70.15, H 4.27, S 5.25.

4,6-Bis(diphenylphosphoryl)dibenzothiophene Sulfone (46DBSODPO). A sample of 0.25 g of white powder with a yield of 40%. ^{1}H NMR (TMS, CDCl$_3$, 400 M Hz): δ = 8.015 (d, J = 7.6 Hz, 2H), 7.697 (m, 10H), 7.614 (t, J = 7.0 Hz, 2H), 7.493 (t, J = 7.0 Hz, 4H), 7.396 ppm (t, J = 7.4 Hz, 8H). LDI-TOF: m/z (%): 616 (100) [M$^+$]; elemental analysis (%) for C$_{36}$H$_{26}$O$_4$P$_2$S: C 70.12, H 4.25, S 5.20; C 70.13, H 4.25, S 5.23.

3,7-Dibromodibenzothiophene Sulfone (37DBSOBr$_2$). At 0 °C, 0.216 g of dibenzothiophene S,S-dioxide (**DBSO**, 1 mmol) was

DOI: 10.1021/acs.chemmater.5b02012
Chem. Mater. XXXX, XXX, XXX−XXX

dissolved in 7.0 mL of H_2SO_4, and then 0.36 g (2 mmol) of NBS was added to the mixture and stirred for 10 h. The reaction was quenched by addition of water (4 mL) and extracted by dichloromethane (3 × 2 mL). The organic layer was dried with anhydride Na_2SO_4. The solvent was removed in vacuo. The residue was purified by flash column chromatography to afford 0.2 g of white powder with a yield of 45%. ^{1}H NMR (TMS, $CDCl_3$, 400 M Hz): δ = 7.943 (s, 2H), 7.786 (d, J = 8.4 Hz, 2H), 7.634 ppm (d, J = 8.0 Hz, 2H). LDI-TOF: m/z (%): 374 (100) [M^+]; elemental analysis (%) for $C_{12}H_6Br_2O_2S$: C 38.53, H 1.62, S 8.57; C 38.55, H 1.61, S 8.64.

3,7-Bis(diphenylphosphoryl)dibenzothiophene Sulfone (37DBSODPO). The procedure was similar to that of **28DBTDPO** except for the use of **37DBSOBr$_2$** (0.374 g, 1 mmol) instead of **28DBTBr$_2$**. Yield: 0.3 g of white powder (49%). ^{1}H NMR (TMS, $CDCl_3$, 400 M Hz): δ = 8.183 (t, J = 9.4 Hz, 2H), 7.966 (t, J = 9.8 Hz, 4H), 7.672 (q, J_1 = 7.0, J_2 = 12.2 Hz, 8H), 7.612 (t, J = 7.4 Hz, 4H), 7.521 ppm (t, J = 7.4 Hz, 8H). LDI-TOF: m/z (%): 616 (100) [M^+]; elemental analysis (%) for $C_{36}H_{26}O_4P_2S$: C 70.12, H 4.25, S 5.20; C 70.11, H 4.27, S 5.28.

DFT Calculations. DFT computations were carried out with different parameters for structure optimizations and vibration analyses. The ground states and triplet states of molecules in vacuum were optimized according to single-crystal structures by the restricted and unrestricted formalism of Beck's three-parameter hybrid exchange functional[41] and Lee, and Yang and Parr correlation functional[42] (B3LYP)/ 6-31G(d), respectively. The charged triplet states with spin multiplicity of 4 were chosen to simplify the calculation on the basis of optimized triplet state configurations. The fully optimized stationary points were further characterized by harmonic vibrational frequency analysis to ensure that real local minima had been found without imaginary vibrational frequency. The total energies were also corrected by zero-point energy both for the ground state and triplet state. The spin density distributions were visualized with Gaussview 3.0. All computations were performed using the Gaussian 03 package.[43]

Device Fabrication and Testing. Before being loaded into a deposition chamber, the ITO substrate was cleaned with detergents and deionized water, dried in an oven at 120 °C for 4 h, and treated with oxygen plasma for 3 min. Devices were fabricated by evaporating organic layers at a rate of 0.1−0.2 nm s^{-1} onto the ITO substrate sequentially at a pressure below 4 × 10^{-4} Pa. Onto the electron-transporting layer, a layer of LiF with 1 nm thickness was deposited at a rate of 0.1 nm s^{-1} to improve electron injection. Finally, a 100 nm-thick layer of Al was deposited at a rate of 0.6 nm s^{-1} as the cathode. The emission area of the devices was 0.09 cm^2, as determined by the overlap area of the anode and the cathode. After fabrication, the devices were immediately transferred to a glovebox for encapsulation with glass coverslips using epoxy glue. The EL spectra and CIE coordinates were measured using a PR650 spectra colorimeter. The current-density−voltage and brightness−voltage curves of the devices were measured using a Keithley 4200 source meter and a calibrated silicon photodiode. All the easurements were carried out at room temperature under ambient conditions. For each structure, five devices were fabricated to confirm the performance repeatability. To make conclusions reliable, the data reported herein were most close to the average results.

3. RESULTS AND DISCUSSIONS

3.1. Design and Structural Compatibility. When T_1 energy of host was equivalent or only slightly higher than that of dopant, the uniform distribution of dopant in host matrix at molecular level would shorten the average distance and time for host−dopant triplet energy transfer, thereby improving the utilization of triplet exciton, besides reducing CQ and TTA to the greatest extent. In this regard, although T_1 value of **DBTDPO** is only 2.91 eV,[40] according to similarity−intermiscibility theory, it was employed as host for **DMAC-DPS** on account of their similar V-shaped configurations and molecular polarities of ∼4.3 D, which can make dispersion of **DMAC-DPS** in **DBTDPO** uniform during evaporation and deposition (Figure 1). Direct evidence was established by atom force microscopy (AFM) images of vacuum-evaporated thin films of **DBTDPO** and **DBTDPO:DMAC-DPS** (10 wt %), which revealed the identical surface morphologies and RMS roughness as small as ∼0.25 nm (Figure 2). In contrast, the

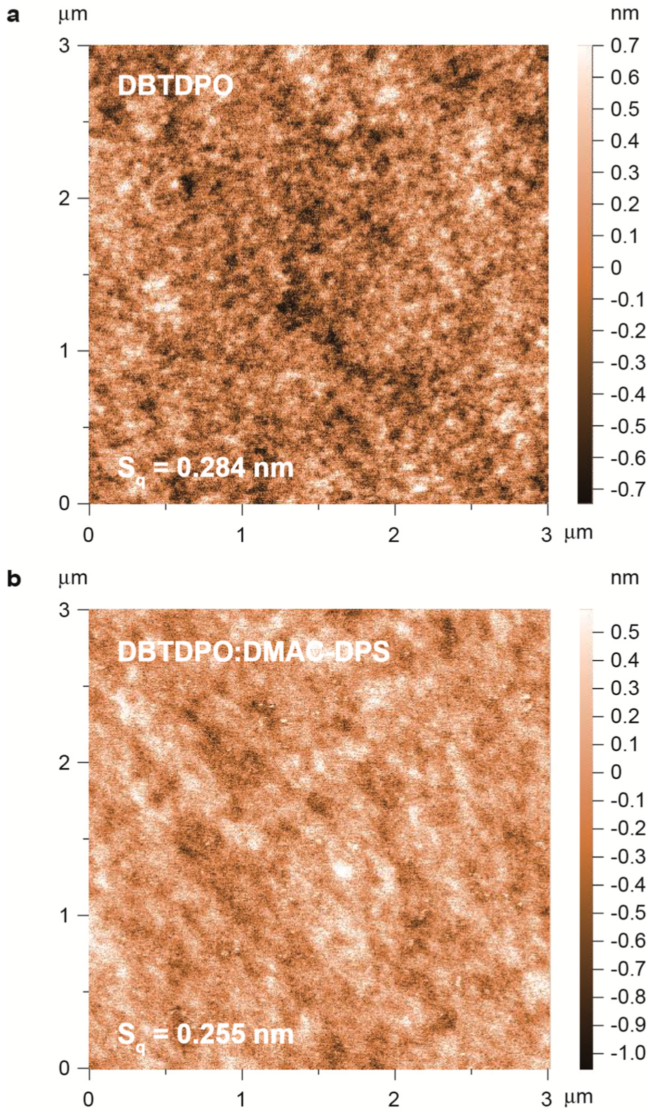

Figure 2. AFM images of 100 nm vacuum-evaporated thin films of neat (a) **DBTDPO** and (b) **DBTDPO:DMAC-DPS** (10 wt %).

neat **DMAC-DPS** film showed the remarkably larger roughness of ∼10 nm due to the strong intermolecular interaction induced crystallization and aggregation (Figure S1, Supporting Information).

Oxidation of sulfur atom in electron-donating dibenzothiophene (**DBT**) can generate strong electron-withdrawing dibenzothiophene sulfone (**DBSO**) without changing molecular configuration, which inspired us to utilize the S,S-dioxide of **DBTDPO**, namely **46DBSODPO**, as ETM, in virtue of their compatibility for modifying EML|ETL interface. As expected, the single-crystal structures of **DBTDPO** and **46DBSODPO** show their identical V-shaped molecular configurations and monoclinic crystal systems, providing the similar packing modes (Figure 1). Obviously, the high consistency of

DOI: 10.1021/acs.chemmater.5b02012
Chem. Mater. XXXX, XXX, XXX−XXX

DBTDPO and **46DBSODPO** in crystallography is beneficial to improve their interface during device fabrication. In contrast, **37DBSODPO** has the same crystal system but different molecular configuration, while **28DBSODPO** shows the similar V-shape configuration but distinct orthorhombic crystal system. Therefore, it is rational that the order of structural compatibility between ***m*DBSODPO** (collective name of **28DBSODPO**, **37DBSODPO**, and **46DBSODPO**) and **DBTDPO** is **46DBSODPO** > **37DBSODPO** > **28DBSODPO**.

3.2. Optical Properties. The PL spectrum of the vacuum-evaporated thin film for **DBTDPO:DMAC-DPS** (10 wt %) consists of the pure emission from **DMAC-DPS** with peak at 482 nm and high PLQY of 87%, which is attributed to the large overlap between PL emission of **DBTDPO** and absorption of **DMAC-DPS** for efficient positive energy transfer (Figure 3a).

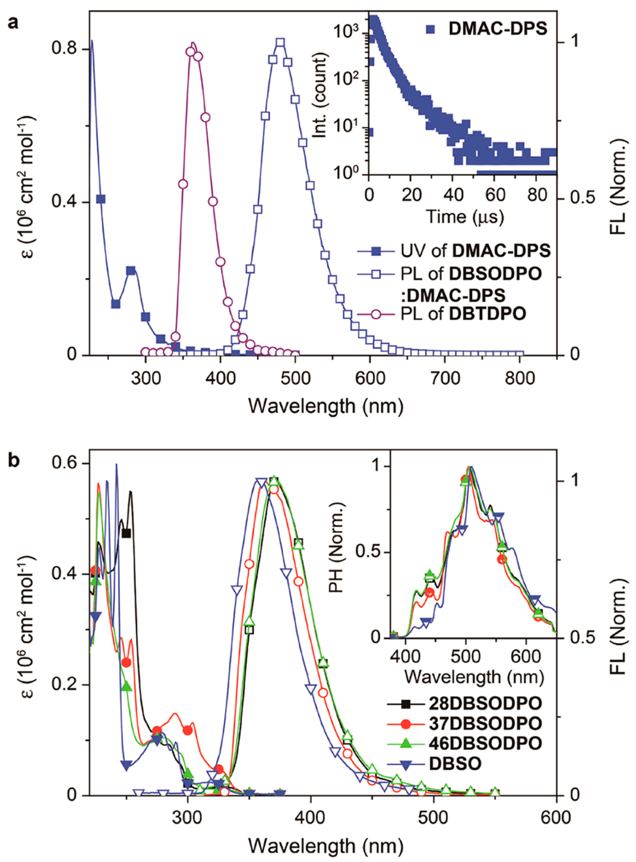

Figure 3. (a) UV absorption spectrum of **DMAC-DPS**, PL spectrum of **DBTDPO**, and steady-state and time-resolved (inset) emission spectra of **DMAC-DPS** in **DBTDPO:DMAC-DPS** (10 wt %) thin film. (b) Electronic absorption and fluorescence (FL) spectra of ***m*DBSODPO** in CH_2Cl_2 (10^{-6} mol L^{-1}) and low-temperature phosphorescence (PH) spectra (inset) by time-resolved technology after a delay of 300 μs, in contrast to **DBSO**.

The transient PL spectrum of the emission at 482 nm shows the remarkable delayed fluorescence component with a long lifetime (τ_{DF}) of 11.5 μs, which is almost four-fold that of **DMAC-DPS** in a conventional host 1,3-bis(9H-carbazol-9-yl)benzene (***m*CP**, τ_{DF} = 3.1 μs, T_1 = 2.9 eV). Although the T_1 energies of **DBTDPO**, ***m*CP**, and **DMAC-DPS** are almost equivalent, the T_1 state of **DMAC-DPS** can be effectively stabilized when doped in **DBTDPO**. The contribution of delayed fluorescence to PLQY is consequently improved to 66%, which is about 10% larger than that of ***m*CP:DMAC-DPS** system. ***m*DBSODPO** reveals similar optical properties in dilute solutions (10^{-6} mol L^{-1} in CH_2Cl_2, Figure 3b and Table 1). **DBSO**-originated bands are preserved in the absorption spectra of ***m*DBSODPO** with bathochromic shifts around 5−15 nm accompanied by diphenylphospohine oxide (DPPO)-attributed peaks at 228 nm. The first singlet excited energy levels (S_1) of ***m*DBSODPO** are identical as 3.41 eV, estimated by their absorption edges at 363 nm. Their fluorescence spectra in solution are also slightly red-shifted in comparison with that of **DBSO**, while the phosphorescence spectra of ***m*DBSODPO** and **DBSO** are identical in both profile and range, in accord with the same locations of their T_1 states on **DBSO** (Figure S1). Their first phosphorescent peaks of 0−0 transitions at 418 nm correspond to higher T_1 values of 2.97 eV. In this case, triplet exciton diffusion from EML of **DBTDPO:DMAC-DPS** to ETL of ***m*DBSODPO** can be blocked.

The intermolecular charge transfer (ICT) between **DBTDPO** and strongly electron-withdrawing ***m*DBSOPO** at the interface between EML and ETL should be considered, which can give rise to the formation of low-energy exciplex,[46] thereby worsening the interfacial quenching of triplet exciton. The exciplex formation between **DBTDPO** and ***m*DBSODPO** was experimentally manifested by the almost identical bathochromic emissions in the range of 350−550 nm in PL spectra of their mixtures in CH_2Cl_2 (Figure 4a). Nevertheless, since ICT on the basis of donor−acceptor collision, is different with the larger molecular degree of freedom in solution for more sufficient intermolecular interactions, in solid states, the steric effects of peripheral groups on intermolecular interactions become predominant. With this consideration, monolayer and bilayer thin films of ***m*DBSODPO** and ***m*DBSODPO|DBTDPO** were prepared through vacuum deposition on quartz substrates to simulate the interfacial interaction in the devices. Compared to PL spectrum of the monolayer film for **28DBSODPO**, a distinct long tail in the spectrum of its bilayer film in the range of 425−550 nm is consistent with exciplex emission of **28DBSODPO:DBTDPO** in solution, verifying the formation of interfacial exciplex (Figure 4b). Contrarily, the tailing peaks in PL spectra of bilayer films for **37DBSODPO** and **46DBSODPO** are either reduced or negligible. Since electron is mainly captured by **DBSO** cores of ***m*DBSOPO**, it is rational that the suppression of exciplex formation is directly proportional to the encapsulation degree of their **DBSO** cores, namely **46DBSODPO** > **37DBSODPO** > **28DBSODPO**, just contrary to the order of their electron mobility.

3.3. Electrical Properties. The electrochemical properties of ***m*DBSODPO** were investigated with CV analysis to figure out the influence of DPPO-substitution on frontier molecular orbital (FMO) energy levels of **DBSO** (Figure 5a and Table 1). The onset potentials of the irreversible oxidation peaks for ***m*DBSODPO** were identical to that of **DBSO** as 1.78 V, corresponding to their highest occupied molecular orbital (HOMO) levels of −6.56 eV. The reduction curves of **28DBSODPO** and **37DBSODPO** consisted of one reversible and one irreversible cathodic peak, while **46DBSODPO** revealed two irreversible reduction peaks, in contrast with one irreversible peak of **DBSO**. Therefore, the lowest unoccupied molecular orbital (LUMO) energy levels of **28DBSODPO**, **37DBSODPO**, and **46DBSODPO** are reduced to −3.46, −3.54, and −3.22 eV, respectively, indicating the order of their electron injection ability as **37DBSODPO** > **28DBSODPO** > **46DBSODPO**, which is consistent with the involvement degrees of their DPPO-substituted C atoms in the

DOI: 10.1021/acs.chemmater.5b02012
Chem. Mater. XXXX, XXX, XXX−XXX

Table 1. Physical Properties of *m*DBSODPO

compound	absorption (nm)	emission[c] (nm)	S_1 (eV)	T_1 (eV)	$T_g/T_m/T_d$ (°C)	HOMO (eV)	LUMO (eV)	RE[g] (eV)	μ_e[h] (cm^2/V/s)
DBSO	324, 291, 278, 269, 242, 234, 228[a]	358[a]	3.60[c]	3.00[e]	−/−/207	−6.56[f]	−3.08[f]	0.4261	
	337, 283, 205[b]	402[b]	4.85[d]	2.86[d]		−6.67[d]	−1.82[d]		
28DBSODPO	333, 284, 249, 240, 227[a]	371[a]	3.41[c]	2.97[e]	−/311/456	−6.56[f]	−3.46[f]	0.5159	7.02×10^{-4}
	337, 295, 286, 276, 258[b]	375[b]	4.68[d]	2.79[d]		−6.84[d]	−2.16[d]		
37DBSODPO	329, 304, 289, 253, 245, 227[a]	362[a]	3.41[c]	2.97[e]	−/−/481	−6.56[f]	−3.54[f]	0.5603	1.56×10^{-4}
	331, 307, 294, 251, 249[b]	385, 368[b]	4.58[d]	2.76[d]		−6.80[d]	−2.22[d]		
46DBSODPO	330, 295, 282, 248, 228[a]	372[a]	3.41[c]	2.97[e]	−/353/459	−6.56[f]	−3.22[f]	0.5736	3.65×10^{-5}
	337, 297, 281, 253[b]	372[b]	4.72[d]	2.85[d]		−6.52[d]	−1.80[d]		

[a]In CH_2Cl_2 (10^{-6} mol L^{-1}). [b]In film. [c]Estimated according to the absorption edges. [d]DFT calculated results. [e]Calculated according to the 0−0 transitions of the phosphorescence spectra. [f]Calculated according to the equation, HOMO/LUMO = 4.78 + onset voltage.[44] [g]Reorganization energy of electron. [h]Electron mobility estimated by $I-V$ characteristics of electron-only devices according filed-dependent SCLC model.[45]

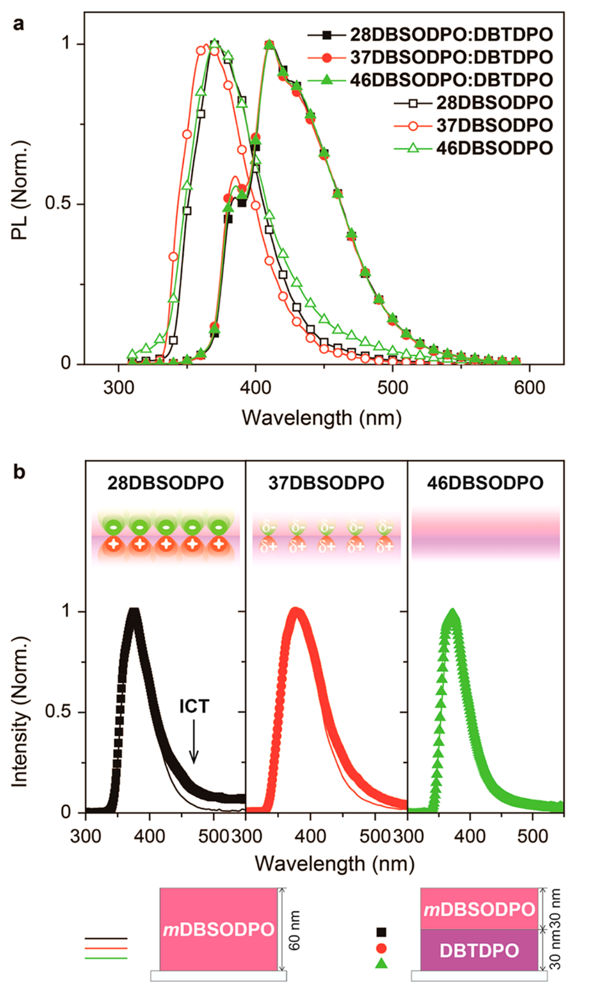

Figure 4. (a) PL spectra of ***m*DBSODPO** (10^{-3} M) before (hollow symbols) and after (solid symbols) addition of **DBTDPO** (0.1 M); (b) PL spectra of vacuum-evaporated monolayer and bilayer thin films of ***m*DBSODPO** (lines) and ***m*DBSODPO|DBTDPO** (symbols). The thickness for each layer of double-layer films was 30 nm, making the whole film thickness equivalent to those of single-layer neat films. ICT refers to intermolecular charge transfer.

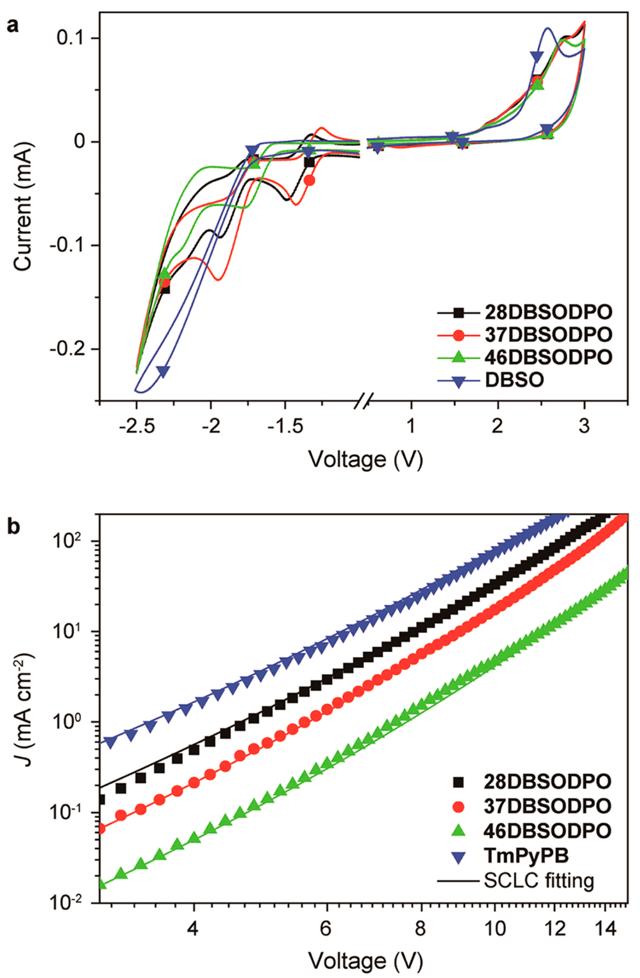

Figure 5. (a) Cyclic voltammograms of ***m*DBSODPO** and **DBSO** measured in CH_2Cl_2 at room temperature with tetrabutylammonium hexafluorophosphate (0.1 M) as electrolyte under the scanning rate of 100 mV s^{-1}; (b) volt−ampere characteristics of ***m*DBSODPO**-based electron-only devices in comparison with those of **TmPyPB**.

LUMOs (Figure S2). The electrochemical stability of ***m*DBSODPO** was further manifested by their stable peaks during 10 reduction cycles (Figure S3), which reflected their device stability. The electron transporting abilities of ***m*DBSODPO** were evaluated by $I-V$ characteristics of their single-layer electron-only devices (Figure 5b and Table 1). The electron mobilities of **28DBSODPO**, **37DBSODPO**, and **46DBSODPO** were estimated as 7.02×10^{-4}, 1.56×10^{-4}, and 3.65×10^{-5} cm^2 V^{-1} s^{-1} according to field-dependent space charge limited current (SCLC) model,[45] which was lower than that of **TmPyPB** as 2.93×10^{-3} cm^2 V^{-1} s^{-1}. **DBSO** cores form the main channel for intermolecular electron hopping

DOI: 10.1021/acs.chemmater.5b02012
Chem. Mater. XXXX, XXX, XXX−XXX

since they make the major contributions to the unoccupied molecular orbitals of ***m*DBSODPO** (Figure S2). In this case, it is rational that the electron mobility of ***m*DBSODPO** is in direct proportion to the exposure degree of their **DBSO** cores, namely **28DBSODPO** > **37DBSODPO** > **46DBSODPO**.

3.4. EL Performance of Blue TADF Diodes. To figure out the significance of the intralayer and interlayer compatibilities on device performance, **DMAC-DPS**-based blue TADF diodes using **DBTDPO** as host and ***m*DBSOPO** as ETL, respectively, were fabricated with a four-layer configuration of ITO|MoO_3 (6 nm)|TAPC (70 nm)|**DBTDPO**:**DMAC-DPS** (10%, 20 nm)|**DBTDPO** (10 nm)|***m*DBSOPO** (30 nm)|LiF (1 nm)|Al, in which TAPC is 1,1-bis(di-4-tolylaminophenyl) cyclohexane as hole transporting layer (HTL) (Figure 6). Adoption of TAPC

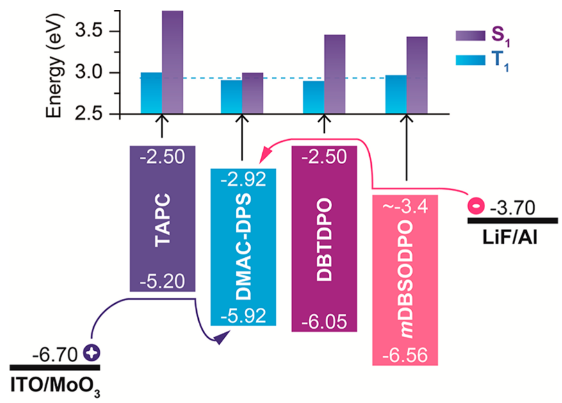

Figure 6. Device configuration of four-layer blue TADF devices and energy level diagram of FMOs and excited states of the employed materials.

is because of its high hole mobility, T_1 value of 2.97 eV, and especially its V-shape configuration to improve interlayer compatibility with EML. If the interfacial effects are not considered, the singlet and triplet excitons can be confined and utilized in EML, in virtue of the higher S_1 and T_1 values of TAPC and ***m*DBSOPO** than those of **DMAC-DPS** (Figure 6). Although T_1 values of **DBTDPO** and **DMAC-DPS** are almost equivalent, the deeper LUMO and shallower HOMO of **DMAC-DPS** formed electron and hole traps with the depths of 0.42 and 0.13 eV for direct charge and exciton capture. Furthermore, the EL spectra of these devices consisted of pure blue-greenish emissions from **DMAC-DPS** with peak wavelength of 476 nm and Commission Internationale de l'Eclairage (CIE) coordinates of (0.16, 0.26), indicating the effective exciton confinement on the dopant (inset of Figure 7a). Because of the low efficiency of **DBTDPO**:***m*DBSODPO** exciplex emissions, which were overlapped with that of **DMAC-DPS**, no distinct exciplex emissions can be observed in EL spectra. However, it can be noticed that the profile of EL spectrum for **28DBSODPO**-based devices was the broadest, which might be attributed to the strongest exciplex emission from **DBTDPO**|**28DBSODPO** interface in accord with PL results.

As expected, **46DBSODPO** endowed its devices with the lowest turn-on voltage less than 3 V at 1 cd m^{-2}, which was even 0.7 V lower than that of **DMAC-DPS**-based six-layer devices (Figure 7a and Table 2). At 150 and 1000 cd m^{-2} for practical applications, the driving voltages were less than 5.5 and 8 V, respectively, which were 1−3 V lower than those of **28DBSODPO** and **37DBSODPO**-based devices; even through

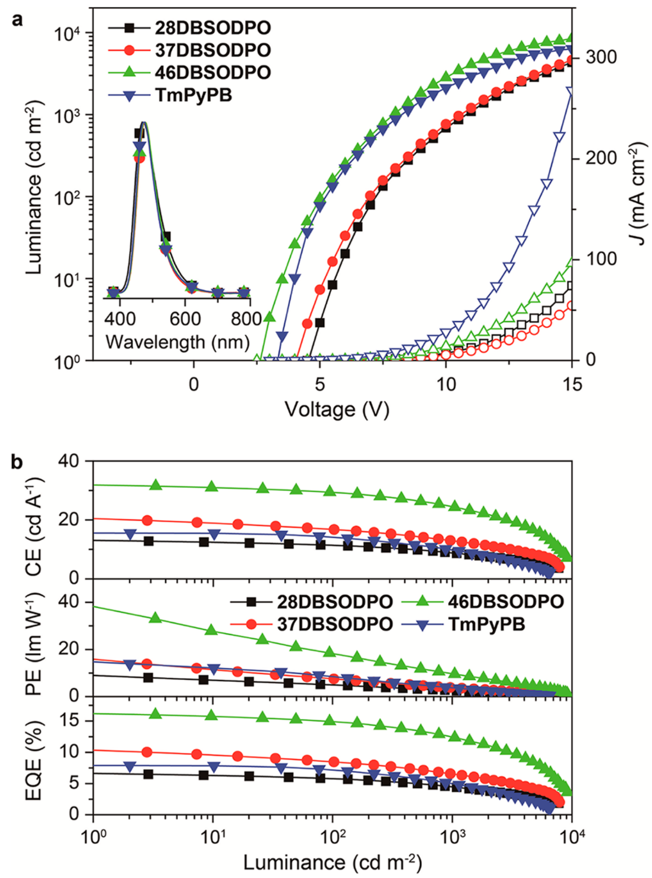

Figure 7. (a) Luminance−current density (*J*)-voltage characteristics and (b) efficiencies−luminance curves of ***m*DBSODPO**-based blue TADF devices in comparison to **TmPyPB**-based controls.

according to CV analysis and *I*−*V* characteristics of electron-only devices, the electron injecting and transporting ability of **46DBSODPO** is the worst among ***m*DBSODPO**. Furthermore, it is noteworthy that the current density (*J*) of **46DBSODPO**-based devices was bigger than those of **28DBSODPO** and **37DBSODPO**-based analogues, reflecting the superior electron injection and transportation in the former. Since **46DBSODPO** is not dominant in intrinsic electrical performance, the reversed *I*−*V* characteristics of these blue TADF diodes should be mainly attributed to interfacial effect and EML−ETL compatibility. The ICT-induced exciplexes of **DBTDPO** and **28DBSODPO** gave rise to the interfacial dipole[47] with positive and negative charges localized on them, respectively, actually forming a built-in field inverted to applied field, which blocked the subsequent electron injection and transportation from cathode (Figure 4b). The situation of **37DBSODPO**-based devices was similar; merely the formation of interfacial exciplex was reduced. Therefore, the superiority of **46DBSODPO** in interfacial exciplex suppression and compatibility with **DBTDPO** should be the main reason for the highest luminance and lowest driving voltage of its devices, which was further verified by the approximate brightness and operation voltages of **TmPyPB**-based devices, in spite of its electron mobility two orders of magnitude larger than that of **46DBSODPO**.

46DBSODPO-based devices showed the state-of-the-art efficiencies with the maxima of 31.5 cd A^{-1} for current efficiency (CE), 32.9 lm W^{1-} for power efficiency (PE), and 16.1% for EQE, which were among the best results for blue TADF devices to date (Figure 7b and Table 2). At 150 cd m^{-2}

DOI: 10.1021/acs.chemmater.5b02012
Chem. Mater. XXXX, XXX, XXX−XXX

Table 2. EL Performance of the Representative Blue TADF Devices

device structure	max. luminance (cd m^{-2})	operating voltage^a (V)	max. efficiencies^b	roll-offs^c (%)		
				CE	PE	EQE
ITO|α-NPD|mCP|DPEPO: CC2BP|DPEPO|TPBi|LiF|Al[31]	3900	4.4	25.5, –, 14.3			
ITO|α-NPD|mCP|mCP: CzTPN|PPT|LiF|Al[32]	16500	4.8, –, –	27.1, 16.7, 11.9			
ITO|α-NPD|mCP|mCP: 2CzPN|PPT|TPBi|LiF|Al[20]			–, –, 13.6			
ITO|PEDOT:PSS|mCP|mCP: DCzIPN|TSPO1|LiF|Al[33]	<5000	3.5, –, –	–, –, 16.4			–, ~54
ITO|α-NPD|TCTA|CzSi|DPEPO: DtBCz-DPS|DPEPO|TPBi|LiF|Al[34]			–, –, 9.9			
ITO|α-NPD|TCTA|CzSi|DPEPO: DMAC-DPS|DPEPO|TPBi|LiF|Al[35]	>10000	3.7, –, –	–, –, 19.5			–, 18
ITO|MoO_3|mCP|DMAC-DPS|DPEPO|LiF|Al[36]	5970	4.3, –, –	–, –, 19.5			
ITO|MoO_3|TAPC|**DBTDPO**:DMAC-DPS|**DBTDPO**|**28DBSOPO**|LiF|Al^d	7754	5.0, <7.5, <11.0	12.8, 8.0, 6.5	15, 32	46, 69	14, 32
ITO|MoO_3|TAPC|**DBTDPO**:DMAC-DPS|**DBTDPO**|**37DBSOPO**|LiF|Al^d	7872	4.5, <7.5, <11.0	19.8, 13.8, 10.1	18, 37	51, 74	18, 37
ITO|MoO_3|TAPC|**DBTDPO**:DMAC-DPS|**DBTDPO**|**46DBSOPO**|LiF|Al^d	9144	3, <5.5, <8.0	31.5, 32.9, 16.1	9, 23	50, 71	9, 23
ITO|MoO_3|TAPC|**DBTDPO**:DMAC-DPS|**DBTDPO**|TmPyPB|LiF|Al^d	6529	3.5, <5.5, <8.5	15.5, 13.9, 7.9	12, 39	44, 75	11, 39

^{a}In the order of onset, 100, and 1000 cd m^{-2}. ^{b}In the order of CE (cd A^{-1}), PE (lm W^{1-}), and EQE (%). ^{c}In the order of 100 and 1000 cd m^{-2}. ^{d}In this work.

for display and 1000 cd m^{-2} for lighting, their EQE values remained as 14.7 and 12.4%, corresponding to reduced efficiency roll-offs of 9 and 23%, respectively. In contrast, the maximum efficiencies of **37DBSODPO**-based devices were remarkably decreased to 19.8 cd A^{-1}, 13.8 lm W^{1-}, and 10.1%, accompanied by worse EQE roll-offs of 18 and 37% at 150 and 1000 cd m^{-2}, respectively. Both **46DBSODPO** and **37DBSODPO** endowed their devices with the efficiencies higher than those of **TmPyPB**-based controls, which should be ascribed to the stronger compatibility of these **DBSO** phosphine oxide derivatives with **DBTDPO**. Furthermore, compared to **DPEPO**-based counterparts with the simplified four-layer structure (Figure S4), **DBTDPO** and **46DBSODPO** supported their devices with remarkably higher luminance and efficiencies, manifesting the significance of intralayer and interlayer compatibility optimization when device simplification for blue TADF diodes. **28DBSODPO**-based devices achieved the maximum efficiencies of only 12.8 cd A^{-1}, 8.0 lm W^{1-}, and 6.5%, which were less than a half of those of **46DBSODPO**-based devices. Consequently, the order of device performances for ***m*DBSODPO** was **46DBSODPO** > **37DBSODPO** > **28DBSODPO**, identical to the order of their compatibility with **DBTDPO** and suppression effect of interfacial exciplex, and contrary to the order of their electrical properties. Actually, in multilayer devices, carrier injection and transportation are not only dependent on intrinsic electrical performances of each involved materials, but also dramatically determined by interfacial effects. Therefore, the optimization of EML/CTL compatibilities is crucial to achieve high EL performance through simple device structures.

4. CONCLUSIONS

In summary, a series of dibenzothiophene-based phosphine oxide materials **DBTDPO** and ***m*DBSODPO** were utilized as host and ETM, respectively, to construct high-efficiency blue TADF devices with simple four-layer configurations. The consistent V-shape configuration and polarity of **DBTDPO** and **DMAC-DPS** and their well-matched optical properties rendered the unchanged morphology and stabilized T_1 states of **DMAC-DPS**-doped thin films with RMS roughness of ~0.25 nm, long τ_{DF} of 11.5 μs, and high PLQY more than 85%. The compatibility between **DBTDPO** and ***m*DBSODPO** was optimized with respect to configuration, packing mode, and interfacial interaction through adjusting the substitution positions of DPPO groups in ***m*DBSODPO**. Although it had inferior in intrinsic electron injecting and transporting ability, **46DBSODPO** endowed its **DMAC-DPS**-based blue TADF devices with the state-of-the-art EQE of 16.1% as maximum and reduced roll-offs of 9 and 23% at 150 and 1000 cd m^{-2}, respectively, owing to its highest compatibility with **DBTDPO** host and the strongest suppression effect on interfacial exciplex. This work shows that besides the intrinsic optoelectronic properties, material compatibility and interfacial optimization should be also concerned for achieving high-performance blue TADF diodes.

■ ASSOCIATED CONTENT

Supporting Information

AFM image of neat **DMAC-DPS** film; energy levels and contours of FMOs and spin-density distributions of the T_1 states of ***m*DBSODPO**; multicyclic reduction curves of ***m*DBSODPO**; and EL performance of **DPEPO**-based control devices. The Supporting Information is available free of charge on the ACS Publications website at DOI: 10.1021/acs.chemmater.5b02012.

■ AUTHOR INFORMATION

Corresponding Authors

*E-mail: hxu@hlju.edu.cn or iamhxu@njtech.edu.cn.
*E-mail: wei-huang@njtech.edu.cn.

Author Contributions

§These authors contributed equally.

Notes

The authors declare no competing financial interest.

■ ACKNOWLEDGMENTS

This project was financially supported by NSFC (61176020 and 51373050), New Century Excellent Talents Supporting Program of MOE (NCET-12-0706), Program for Innovative Research Team in University (MOE) (IRT-1237), Science and Technology Bureau of Heilongjiang Province (ZD201402 and JC2015002), Education Bureau of Heilongjiang Province (2014CJHB005), and the Fok Ying-Tong Education Foundation for Young Teachers in the Higher Education Institutions of China (141012).

■ REFERENCES

(1) Forrest, S. R.; Baldo, M. A.; O'Brien, D. F.; You, Y.; Shoustikov, A.; Sibley, S.; Thompson, M. E. Highly efficient phosphorescent emission from organic electroluminescent device. *Nature* **1998**, *395*, 151−154.

(2) Reineke, S.; Lindner, F.; Schwartz, G.; Seidler, N.; Walzer, K.; Lussem, B.; Leo, K. White organic light-emitting diodes with fluorescent tube efficiency. *Nature* **2009**, *459*, 234−238.

(3) McCarthy, M. A.; Liu, B.; Donoghue, E. P.; Kravchenko, I.; Kim, D. Y.; So, F.; Rinzler, A. G. Low-Voltage, Low-Power, Organic Light-Emitting Transistors for Active Matrix Displays. *Science* **2011**, *332*, 570−573.

(4) Endo, A.; Ogasawara, M.; Takahashi, A.; Yokoyama, D.; Kato, Y.; Adachi, C. Thermally activated delayed fluorescence from Sn(4+)-porphyrin complexes and their application to organic light emitting diodes–a novel mechanism for electroluminescence. *Adv. Mater.* **2009**, *21* (47), 4802−4806.

(5) Tao, Y.; Yuan, K.; Chen, T.; Xu, P.; Li, H.; Chen, R.; Zheng, C.; Zhang, L.; Huang, W. Thermally activated delayed fluorescence materials towards the breakthrough of organoelectronics. *Adv. Mater.* **2014**, *26* (47), 7931−7958.

(6) Dias, F. B.; Bourdakos, K. N.; Jankus, V.; Moss, K. C.; Kamtekar, K. T.; Bhalla, V.; Santos, J.; Bryce, M. R.; Monkman, A. P. Triplet harvesting with 100% efficiency by way of thermally activated delayed fluorescence in charge transfer OLED emitters. *Adv. Mater.* **2013**, *25* (27), 3707−3714.

(7) Leitl, M. J.; Krylova, V. A.; Djurovich, P. I.; Thompson, M. E.; Yersin, H. Phosphorescence versus Thermally Activated Delayed Fluorescence. Controlling Singlet−Triplet Splitting in Brightly Emitting and Sublimable Cu(I) Compounds. *J. Am. Chem. Soc.* **2014**, *136* (45), 16032−16038.

(8) Wang, H.; Xie, L.; Peng, Q.; Meng, L.; Wang, Y.; Yi, Y.; Wang, P. Novel Thermally Activated Delayed Fluorescence Materials−Thioxanthone Derivatives and Their Applications for Highly Efficient OLEDs. *Adv. Mater.* **2014**, *26* (30), 5198−5204.

(9) Sun, J. W.; Lee, J. H.; Moon, C. K.; Kim, K. H.; Shin, H.; Kim, J. J. A fluorescent organic light-emitting diode with 30% external quantum efficiency. *Adv. Mater.* **2014**, *26* (32), 5684−5688.

(10) Liu, X.-K.; Chen, Z.; Zheng, C.-J.; Liu, C.-L.; Lee, C.-S.; Li, F.; Ou, X.-M.; Zhang, X.-H. Prediction and Design of Efficient Exciplex Emitters for High-Efficiency, Thermally Activated Delayed-Fluorescence Organic Light-Emitting Diodes. *Adv. Mater.* **2015**, *27* (14), 2378−2383.

(11) Zhang, D.; Duan, L.; Li, Y.; Zhang, D.; Qiu, Y. Highly efficient and color-stable hybrid warm white organic light-emitting diodes using a blue material with thermally activated delayed fluorescence. *J. Mater. Chem. C* **2014**, *2* (38), 8191−8197.

(12) Yao, L.; Zhang, S.; Wang, R.; Li, W.; Shen, F.; Yang, B.; Ma, Y. Highly efficient near-infrared organic light-emitting diode based on a butterfly-shaped donor-acceptor chromophore with strong solid-state fluorescence and a large proportion of radiative excitons. *Angew. Chem., Int. Ed.* **2014**, *53* (8), 2119−2123.

(13) Li, W.; Pan, Y.; Xiao, R.; Peng, Q.; Zhang, S.; Ma, D.; Li, F.; Shen, F.; Wang, Y.; Yang, B.; Ma, Y. Employing ∼100% Excitons in OLEDs by Utilizing a Fluorescent Molecule with Hybridized Local and Charge-Transfer Excited State. *Adv. Funct. Mater.* **2014**, *24* (11), 1609−1614.

(14) Zheng, C.-J.; Wang, J.; Ye, J.; Lo, M.-F.; Liu, X.-K.; Fung, M.-K.; Zhang, X.-H.; Lee, C.-S. Novel Efficient Blue Fluorophors with Small Singlet-Triplet Splitting: Hosts for Highly Efficient Fluorescence and Phosphorescence Hybrid WOLEDs with Simplified Structure. *Adv. Mater.* **2013**, *25* (15), 2205−2211.

(15) Hofbeck, T.; Monkowius, U.; Yersin, H. Highly Efficient Luminescence of Cu(I) Compounds: Thermally Activated Delayed Fluorescence Combined with Short-Lived Phosphorescence. *J. Am. Chem. Soc.* **2015**, *137* (1), 399−404.

(16) Hu, J.-Y.; Pu, Y.-J.; Satoh, F.; Kawata, S.; Katagiri, H.; Sasabe, H.; Kido, J. Bisanthracene-Based Donor−Acceptor-type Light-Emitting Dopants: Highly Efficient Deep-Blue Emission in Organic Light-Emitting Devices. *Adv. Funct. Mater.* **2014**, *24* (14), 2064−2071.

(17) Zhang, Q.; Kuwabara, H.; Potscavage, W. J., Jr.; Huang, S.; Hatae, Y.; Shibata, T.; Adachi, C. Anthraquinone-based intramolecular charge-transfer compounds: computational molecular design, thermally activated delayed fluorescence, and highly efficient red electroluminescence. *J. Am. Chem. Soc.* **2014**, *136* (52), 18070−18081.

(18) Mayr, C.; Lee, S. Y.; Schmidt, T. D.; Yasuda, T.; Adachi, C.; Brütting, W. Efficiency Enhancement of Organic Light-Emitting Diodes Incorporating a Highly Oriented Thermally Activated Delayed Fluorescence Emitter. *Adv. Funct. Mater.* **2014**, *24* (33), 5232−5239.

(19) Zhang, Q.; Komino, T.; Huang, S.; Matsunami, S.; Goushi, K.; Adachi, C. Triplet Exciton Confinement in Green Organic Light-Emitting Diodes Containing Luminescent Charge-Transfer Cu(I) Complexes. *Adv. Funct. Mater.* **2012**, *22* (11), 2327−2336.

(20) Masui, K.; Nakanotani, H.; Adachi, C. Analysis of exciton annihilation in high-efficiency sky-blue organic light-emitting diodes with thermally activated delayed fluorescence. *Org. Electron.* **2013**, *14* (11), 2721−2726.

(21) Han, C.; Zhu, L.; Li, J.; Zhao, F.; Zhang, Z.; Xu, H.; Deng, Z.; Ma, D.; Yan, P. Highly Efficient Multifluorenyl Host Materials with Unsymmetrical Molecular Configurations and Localized Triplet States for Green and Red Phosphorescent Devices. *Adv. Mater.* **2014**, *26* (41), 7070−7077.

(22) Kan, W.; Zhu, L.; Wei, Y.; Ma, D.; Sun, M.; Wu, Z.; Huang, W.; Xu, H. Phosphine oxide-jointed electron transporters for the reduction of interfacial quenching in highly efficient blue PHOLEDs. *J. Mater. Chem. C* **2015**, *3* (21), 5430−5439.

(23) Baldo, M. A.; Adachi, C.; Forrest, S. R. Transient analysis of organic electrophosphorescence. II. Transient analysis of triplet-triplet annihilation. *Phys. Rev. B: Condens. Matter Mater. Phys.* **2000**, *62* (16), 10967.

(24) Reineke, S.; Walzer, K.; Leo, K. Triplet-exciton quenching in organic phosphorescent light-emitting diodes with Ir-based emitters. *Phys. Rev. B: Condens. Matter Mater. Phys.* **2007**, *75* (12), 125328.

(25) Kim, B. S.; Lee, J. Y. Engineering of Mixed Host for High External Quantum Efficiency above 25% in Green Thermally Activated Delayed Fluorescence Device. *Adv. Funct. Mater.* **2014**, *24* (25), 3970−3977.

(26) Kim, B. S.; Lee, J. Y. Phosphine oxide type bipolar host material for high quantum efficiency in thermally activated delayed fluorescent device. *ACS Appl. Mater. Interfaces* **2014**, *6* (11), 8396−400.

(27) Im, Y.; Lee, J. Y. Above 20% External Quantum Efficiency in Thermally Activated Delayed Fluorescence Device Using Furodipyridine-Type Host Materials. *Chem. Mater.* **2014**, *26* (3), 1413−1419.

(28) Zhang, D.; Duan, L.; Li, C.; Li, Y.; Li, H.; Zhang, D.; Qiu, Y. High-Efficiency Fluorescent Organic Light-Emitting Devices Using Sensitizing Hosts with a Small Singlet−Triplet Exchange Energy. *Adv. Mater.* **2014**, *26* (29), 5050−5055.

(29) Cho, Y. J.; Yook, K. S.; Lee, J. Y. A universal host material for high external quantum efficiency close to 25% and long lifetime in green fluorescent and phosphorescent OLEDs. *Adv. Mater.* **2014**, *26* (24), 4050−4055.

(30) Uoyama, H.; Goushi, K.; Shizu, K.; Nomura, H.; Adachi, C. Highly efficient organic light-emitting diodes from delayed fluorescence. *Nature* **2012**, *492* (7428), 234−238.

(31) Lee, S. Y.; Yasuda, T.; Yang, Y. S.; Zhang, Q.; Adachi, C. Luminous Butterflies: Efficient Exciton Harvesting by Benzophenone Derivatives for Full-Color Delayed Fluorescence OLEDs. *Angew. Chem., Int. Ed.* **2014**, *53* (25), 6402−6406.

(32) Nishimoto, T.; Yasuda, T.; Lee, S. Y.; Kondo, R.; Adachi, C. A six-carbazole-decorated cyclophosphazene as a host with high triplet energy to realize efficient delayed-fluorescence OLEDs. *Mater. Horiz.* **2014**, *1* (2), 264−269.

(33) Cho, Y. J.; Yook, K. S.; Lee, J. Y. Cool and warm hybrid white organic light-emitting diode with blue delayed fluorescent emitter both as blue emitter and triplet host. *Sci. Rep.* **2015**, *5*, 7859.

(34) Zhang, Q.; Li, J.; Shizu, K.; Huang, S.; Hirata, S.; Miyazaki, H.; Adachi, C. Design of efficient thermally activated delayed fluorescence

DOI: 10.1021/acs.chemmater.5b02012
Chem. Mater. XXXX, XXX, XXX−XXX

materials for pure blue organic light emitting diodes. *J. Am. Chem. Soc.* **2012**, *134* (36), 14706−14709.
(35) Zhang, Q.; Li, B.; Huang, S.; Nomura, H.; Tanaka, H.; Adachi, C. Efficient blue organic light-emitting diodes employing thermally activated delayed fluorescence. *Nat. Photonics* **2014**, *8*, 326−332.
(36) Zhang, Q.; Tsang, D.; Kuwabara, H.; Hatae, Y.; Li, B.; Takahashi, T.; Lee, S. Y.; Yasuda, T.; Adachi, C. Nearly 100% Internal Quantum Efficiency in Undoped Electroluminescent Devices Employing Pure Organic Emitters. *Adv. Mater.* **2015**, *27* (12), 2096−2100.
(37) Wu, S. H.; Aonuma, M.; Zhang, Q. S.; Huang, S. P.; Nakagawa, T.; Kuwabara, K.; Adachi, C. High-efficiency deep-blue organic light-emitting diodes based on a thermally activated delayed fluorescence emitter. *J. Mater. Chem. C* **2014**, *2* (3), 421−424.
(38) Chen, X.-L.; Yu, R.; Zhang, Q.-K.; Zhou, L.-J.; Wu, X.-Y.; Zhang, Q.; Lu, C.-Z. Rational Design of Strongly Blue-Emitting Cuprous Complexes with Thermally Activated Delayed Fluorescence and Application in Solution-Processed OLEDs. *Chem. Mater.* **2013**, *25* (19), 3910−3920.
(39) Adachi, C.; Kwong, R. C.; Djurovich, P.; Adamovich, V.; Baldo, M. A.; Thompson, M. E.; Forrest, S. R. [CBP for Blue] Endothermic energy transfer: A mechanism for generating very efficient high-energy phosphorescent emission in organic materials. *Appl. Phys. Lett.* **2001**, *79*, 2082−2084.
(40) Han, C.; Zhang, Z.; Xu, H.; Yue, S.; Li, J.; Yan, P.; Deng, Z.; Zhao, Y.; Yan, P.; Liu, S. Short-Axis Substitution Approach Selectively Optimizes Electrical Properties of Dibenzothiophene-Based Phosphine Oxide Hosts. *J. Am. Chem. Soc.* **2012**, *134* (46), 19179−19188.
(41) Becke, A. D. Density-functional thermochemistry. III. The role of exact exchange. *J. Chem. Phys.* **1993**, *98* (7), 5648−5652.
(42) Lee, C.; Yang, W.; Parr, R. G. Development of the Colle-Salvetti correlation-energy formula into a functional of the electron density. *Phys. Rev. B: Condens. Matter Mater. Phys.* **1988**, *37* (2), 785−789.
(43) Frisch, M. J.; Trucks, G. W.; Schlegel, H. B.; Scuseria, G. E.; Robb, M. A.; Cheeseman, J. R.; Montgomery, J. A., Jr.; Vreven, T.; Kudin, K. N.; Burant, J. C.; Millam, J. M.; Iyengar, S. S.; Tomasi, J.; Barone, V.; Mennucci, B.; Cossi, M.; Scalmani, G.; Rega, N.; Petersson, G. A.; Nakatsuji, H.; Hada, M.; Ehara, M.; Toyota, K.; Fukuda, R.; Hasegawa, J.; Ishida, M.; Nakajima, T.; Honda, Y.; Kitao, O.; Nakai, H.; Klene, M.; Li, X.; Knox, J. E.; Hratchian, H. P.; Cross, J. B.; Bakken, V.; Adamo, C.; Jaramillo, J.; Gomperts, R.; Stratmann, R. E.; Yazyev, O.; Austin, A. J.; Cammi, R.; Pomelli, C.; Ochterski, J. W.; Ayala, P. Y.; Morokuma, K.; Voth, G. A.; Salvador, P.; Dannenberg, J. J.; Zakrzewski, V. G.; Dapprich, S.; Daniels, A. D.; Strain, M. C.; Farkas, O.; Malick, D. K.; Rabuck, A. D.; Raghavachari, K.; Foresman, J. B.; Ortiz, J. V.; Cui, Q.; Baboul, A. G.; Clifford, S.; Cioslowski, J.; Stefanov, B. B.; Liu, G.; Liashenko, A.; Piskorz, P.; Komaromi, I.; Martin, R. L.; Fox, D. J.; Keith, T.; Al-Laham, M. A.; Peng, C. Y.; Nanayakkara, A.; Challacombe, M.; Gill, P. M. W.; Johnson, B.; Chen, W.; Wong, M. W.; Gonzalez, C.; Pople, J. A. *Gaussian 03*, revision D.02; Gaussian, Inc.: Wallingford, CT, 2003.
(44) de Leeuw, D. M.; Simenon, M. M. J.; Brown, A. R.; Einerhand, R. E. F. Stability of n-type doped conducting polymers and consequences for polymeric microelectronic devices. *Synth. Met.* **1997**, *87* (1), 53−59.
(45) Wang, Z. B.; Helander, M. G.; Greiner, M. T.; Qiu, J.; Lu, Z. H. $$$$[mobility]Carrier mobility of organic semiconductors based on current-voltage characteristics. *J. Appl. Phys.* **2010**, *107* (3), 034506.
(46) Hung, W. Y.; Fang, G. C.; Chang, Y. C.; Kuo, T. Y.; Chou, P. T.; Lin, S. W.; Wong, K. T. Highly efficient bilayer interface exciplex for yellow organic light-emitting diode. *ACS Appl. Mater. Interfaces* **2013**, *5* (15), 6826−6831.
(47) Osikowicz, W.; de Jong, M. P.; Salaneck, W. R. Formation of the Interfacial Dipole at Organic-Organic Interfaces: C60/Polymer Interfaces. *Adv. Mater.* **2007**, *19* (23), 4213−4217.

DOI: 10.1021/acs.chemmater.5b02012
Chem. Mater. XXXX, XXX, XXX−XXX